Neurobiology of Disease 130 (2019) 104534

Contents lists available at ScienceDirect

Neurobiology of Disease

journal homepage: www.elsevier.com/locate/ynbdi

# Non-genetically modified models exhibit *TARDBP* mRNA increase due to perturbed TDP-43 autoregulation

Akihiro Sugai[a], Taisuke Kato[b], Akihide Koyama[c], Yuka Koike[a], Takuya Konno[a], Tomohiko Ishihara[d], Osamu Onodera[a,*]

[a] Department of Neurology, Clinical Neuroscience Branch, Brain Research Institute, Niigata University, Niigata 951-8585, Japan
[b] Department of System Pathology for Neurological Disorders, Brain Science Branch, Center for Bioresource-based Research, Brain Research Institute, Niigata University, Niigata 951-8585, Japan
[c] Division of Legal Medicine, Graduate School of Medicine and Dental Science, Niigata University, Niigata 951-8585, Japan
[d] Department of Molecular Neuroscience, Resource Branch for Brain Disease Research, Center for Bioresource-based Research, Brain Research Institute, Niigata University, Niigata 951-8585, Japan

ARTICLE INFO

*Keywords:*
Amyotrophic lateral sclerosis
TDP-43
autoregulation
alternative splicing
antisense oligonucleotides

ABSTRACT

Amyotrophic lateral sclerosis (ALS) is a neurodegenerative disease characterized by accumulation of fragmented insoluble TDP-43 and loss of TDP-43 from the nucleus. Increased expression of exogenous *TARDBP* (encoding TDP-43) induces TDP-43 pathology and cytotoxicity, suggesting the involvement of aberrant expression of TDP-43 in the pathogenesis of ALS. In normal conditions, however, the amount of TDP-43 is tightly regulated by the autoregulatory mechanism involving alternative splicing of *TARDBP* mRNA. To investigate the influence of autoregulation dysfunction, we inhibited the splicing of cryptic intron 6 using antisense oligonucleotides *in vivo*. This inhibition doubled the *Tardbp* mRNA expression, increased the fragmented insoluble TDP-43, and reduced the number of motor neurons in the mouse spinal cord. In human induced pluripotent stem cell-derived neurons, the splicing inhibition of intron 6 increased *TARDBP* mRNA and decreased nuclear TDP-43. These non-genetically modified models exhibiting rise in the *TARDBP* mRNA levels suggest that TDP-43 autoregulation turbulence might be linked to the pathogenesis of ALS.

## 1. Introduction

Amyotrophic lateral sclerosis (ALS) is a fatal neurodegenerative disease that causes the progressive loss of motor neurons. In the affected neurons of patients with ALS, TAR DNA binding protein 43 (TDP-43) disappears from the nucleus, phosphorylates, fragments, and forms inclusions in the cytoplasm (Arai et al., 2006; Neumann et al., 2006). Mutations in the *TARDBP* gene encoding TDP-43 cause familial ALS, with pathology similar to sporadic ALS (Sreedharan et al., 2008; Yokoseki et al., 2008), indicating that TDP-43 is directly involved in the pathogenesis of ALS. TDP-43 is a nuclear RNA binding protein with a prion-like domain (Ling et al., 2013; Ratti and Buratti, 2016) and an excess of exogenous TDP-43 induces cytotoxicity and TDP-43 pathology mimicking ALS (Ke et al., 2015; Tsai et al., 2010; Walker et al., 2015; Xu et al., 2010). We therefore speculate that the mechanism by which endogenous TDP-43 protein is increased might underlie the pathogenesis of ALS.

In normal conditions, the amount of TDP-43 is tightly auto-regulated via processing of *TARDBP* transcripts (Ayala et al., 2011; Polymenidou et al., 2011). *TARDBP* has at least two cryptic introns and three polyadenylation signals in the last gigantic exon. Nuclear TDP-43 decreases normal *TARDBP* mRNA and increases mRNA susceptible to nonsense-mediated mRNA decay (NMD) by promoting splicing of cryptic introns, and as a result, the TDP-43 protein decreases. In contrast, depletion of nuclear TDP-43 suppresses splicing of cryptic introns and increases canonical *TARDBP* mRNA, inducing TDP-43 protein expression (Koyama et al., 2016). Indeed, transcription of *TARDBP* mRNA is redundant, and about 50% of the transcribed mRNA is degraded (Sugai et al., 2018). We have thus proposed that the robustness of the regulation of the amount of TDP-43 is based on the transcriptional redundancy of *TARDBP* mRNA (Sugai et al., 2018).

Using an *in silico* model, we noticed that the robustness of TDP-43

*Abbreviations:* ALS, amyotrophic lateral sclerosis; TDP-43, TAR DNA binding protein 43; NMD, nonsense-mediated mRNA decay; iPSC, induced pluripotent stem cell; ASO, antisense oligonucleotides

* Corresponding author.
*E-mail address:* onodera@bri.niigata-u.ac.jp (O. Onodera).

https://doi.org/10.1016/j.nbd.2019.104534
Received 18 October 2018; Received in revised form 22 June 2019; Accepted 12 July 2019
Available online 13 July 2019

autoregulation is vulnerable to several factors involved in the function of ALS-related genes (Sugai et al., 2018). The decrease in the efficiency of TDP-43 autoregulation itself was one of factors that made the system vulnerable. Thus, we have speculated that an increase in *TARDBP* mRNA based on transcriptional redundancy triggered by these factors causes a vicious circle leading to TDP-43 pathology. In this process, splicing of cryptic introns is suppressed and canonical *TARDBP* mRNA increases. Indeed, we found a decrease in alternative splicing of *TARDBP* mRNA in ALS spinal cords and an increase in cytoplasmic *TARDBP* mRNA in ALS-affected motor neurons (Koyama et al., 2016). In addition, in a *Tardbp* knock-in mouse model with an ALS-causative gene mutation, splicing of cryptic intron 7 decreases and the amount of *Tardbp* mRNA and TDP-43 protein increases (Fratta et al., 2018; White et al., 2018). However, it has not been clarified whether disorder of alternative splicing of *TARDBP* mRNA, as a primary factor, causes an increase in TDP-43, ALS-relevant TDP-43 pathology, and loss of motor neurons *in vivo*.

In this study, we sought to increase TDP-43 by suppressing alternative splicing of *TARDBP* mRNA in mouse spinal motor neurons and human neurons derived from induced pluripotent stem cell. To inhibit the alternative splicing, we used antisense oligonucleotides that target the splicing sites of cryptic introns. We then investigated whether turbulence of the autoregulatory mechanism by alternative splicing inhibition causes ALS-related pathology.

## 2. Materials & methods

### 2.1. Antisense oligonucleotides (ASO)

Morpholino antisense oligonucleotides (ASO) targeting each cryptic intron splicing site of *TARDBP* pre-mRNA was designed and synthesized by GeneTools (Oregon, USA). Standard Control Morpholino Oligo (GeneTools) was used for control ASO (ASO-ctrl). For administration to mice, morpholino ASO conjugated with octa-guanidine dendrimer (Vivo-Morpholinos; Gene tools) was used. Supp. Table 1 shows the ASO sequence.

### 2.2. Administration of ASO into the cerebrospinal space of mice

Male C57BL/6NCrl mice aged 11–12 weeks or 17–18 months old were anesthetized by intraperitoneal injection of chloral hydrate (350 mg/kg) and xylazine (10 mg/kg). A longitudinal incision was made in the skin of the middle of the lumbar region of the mouse. A 32-gauge needle attached to one end of a PE-10 polyethylene tube was inserted into the cerebrospinal space between the fifth and sixth lumbar vertebrae. The correct position of the top of the needle was confirmed by slight cerebrospinal fluid backflow to the polyethylene tube through application of negative pressure. Mice were excluded from the study when blood contamination was observed in the polyethylene tube. Then 7 µl Vivo-Morpholinos (1.5 µg or 3.0 µg) diluted with artificial cerebrospinal fluid was injected at a rate of 0.1 µl/min. The artificial cerebrospinal fluid contained Na 150 mM, K 3.0 mM, Ca 1.4 mM, Mg 0.8 mM, P 1.0 mM, and Cl 155 mM. Due to the toxicity of Vivo-Morpholinos (Zhou et al., 2013), dysuria was observed in all mice, but no apparent behavioral sequelae—including movement and feeding abnormalities due to intrathecal injection—were observed. The Institutional Animal Care and Use Committee of Niigata University approved this animal experiment.

### 2.3. RNA extraction and reverse transcription PCR

For analysis of the mouse spinal cord, one side of the resected spinal cord was used for RNA extraction and the other side was used for protein extraction. Total RNA was extracted using Nucleospin RNA II (Takara Bio). First-strand cDNA was synthesized using ReverTra Ace (TOYOBO). PCR was performed using LA Taq polymerase (Takara Bio). PCR amplification products were separated by electrophoresis using a 2% agarose gel, and the band intensity was quantified using a LAS 4000 mini biomolecular imager (GE Healthcare). Quantitative real-time PCR was performed on the TP-850 Real-Time PCR Detection System (Takara Bio) using SYBR Green Premix ExTaq II. Quantitative real-time PCR conditions were 95 °C for 30 s for initial denaturation, followed by 40 cycles of 95 °C for 5 s and 60 °C for 30 s. Relative expression of target mRNA was calculated using the ΔΔCT method. Supp. Tables 2 and 3 show the primer sequence.

### 2.4. Protein extraction from mouse spinal cord and western blotting

The mouse lumbar spinal cord was immersed and pulverized in 400 µl RIPA buffer (25 mM Tris-HCl pH 7.6, 150 mM NaCl, 1% NP-40, 1% sodium deoxycholate, 0.1% SDS) supplemented with protease inhibitor cocktail (Sigma) and phosphatase inhibitor cocktail (Sigma). The lysate was sonicated on ice and centrifuged at 100,000 ×*g* at 4 °C for 30 min. The supernatant was used as a RIPA soluble fraction. To ensure removal of all RIPA soluble proteins, the operation of dissolving the pellet in RIPA buffer, sonicating, and centrifuging at 100,000 ×*g* for 30 min at 4 °C was repeated twice. The insoluble pellet was dissolved in 100 µl urea buffer (7 M urea, 2 M thiourea, 4% CHAPS, and 30 mM Tris, pH 8.5) supplemented with protease inhibitor cocktail and phosphatase inhibitor cocktail, sonicated, and centrifuged at 100,000 ×*g* at 22 °C for 30 min. The supernatant was used as the urea-soluble fraction. The protein concentration of the RIPA soluble fraction was measured using the BCA protein assay kit (Thermo). The protein concentration of the urea fraction was assumed to have the same ratio as that of the RIPA soluble fraction.

The supernatant was resuspended in Laemmli Sample Buffer (BioRad) and treated at 96 °C for 5 min. Proteins were separated by SDS-PAGE using 10% polyacrylamide gel (Super SepTM Ace, Wako) and transferred to a PVDF membrane (Millipore). The blot was immersed in the primary antibody overnight at 4 °C. Antibodies used for immunoblotting were rabbit anti-TDP-43 (C-Terminal) polyclonal antibody (Proteintech 12892-1-AP), rabbit anti-TDP-43 (N-Terminal) polyclonal antibody (Proteintech 10782-2-AP), rabbit anti-BIM monoclonal antibody (C34C5, Cell Signaling Technology), and mouse anti-GAPDH monoclonal antibody (MBL). HRP-conjugated secondary antibodies (Dako) were used. Bands were detected using Immobilon Western Chemiluminescent HRP Substrate (Millipore) and were quantitatively analyzed using ImageQuant™ LAS 4000 biomolecular imager (GE Healthcare).

### 2.5. Laser capture microdissection

The lumbar spinal cord of the mouse was divided transversely into 4 pieces. These tissues were embedded in OCT compound, and snap-frozen in 2-methylbutane precooled with liquid nitrogen. The OCT embedded block was cryosectioned at a thickness of 14 µm on 2.0 mm PEN-Membrane slides (Leica) and dried under a stream of cool air for 2 min. The dried slides were incubated as follows: (1) 95% ethanol for 1 min, (2) 75% ethanol for 1 min, (3) 1% Cresyl violet in 75% ethanol for 2 min, (4) 75% ethanol for 30 s, (5) 95% ethanol for 30 s, (6) 100% ethanol for 30 s, twice, and (7) 100% ethanol for 5 min. The stained 160 motor neurons per mouse or posterior horns were incised with LEICA 700DMB (Leica) and were dissolved in Lysis buffer (RNAqueous-Micro Kit, Ambion). RNA was extracted using RNAqueous-Micro Kit (Ambion).

### 2.6. Immunofluorescent staining of mouse spinal cord

Sections 4 µm thick from the paraffin-embedded specimens were deparaffinized and rehydrated. For antigen unmasking, the sections were boiled in 10 mM sodium citrate buffer (pH 6.0). Sections were blocked and permeabilized with 0.1% Triton X-100 and 5% bovine

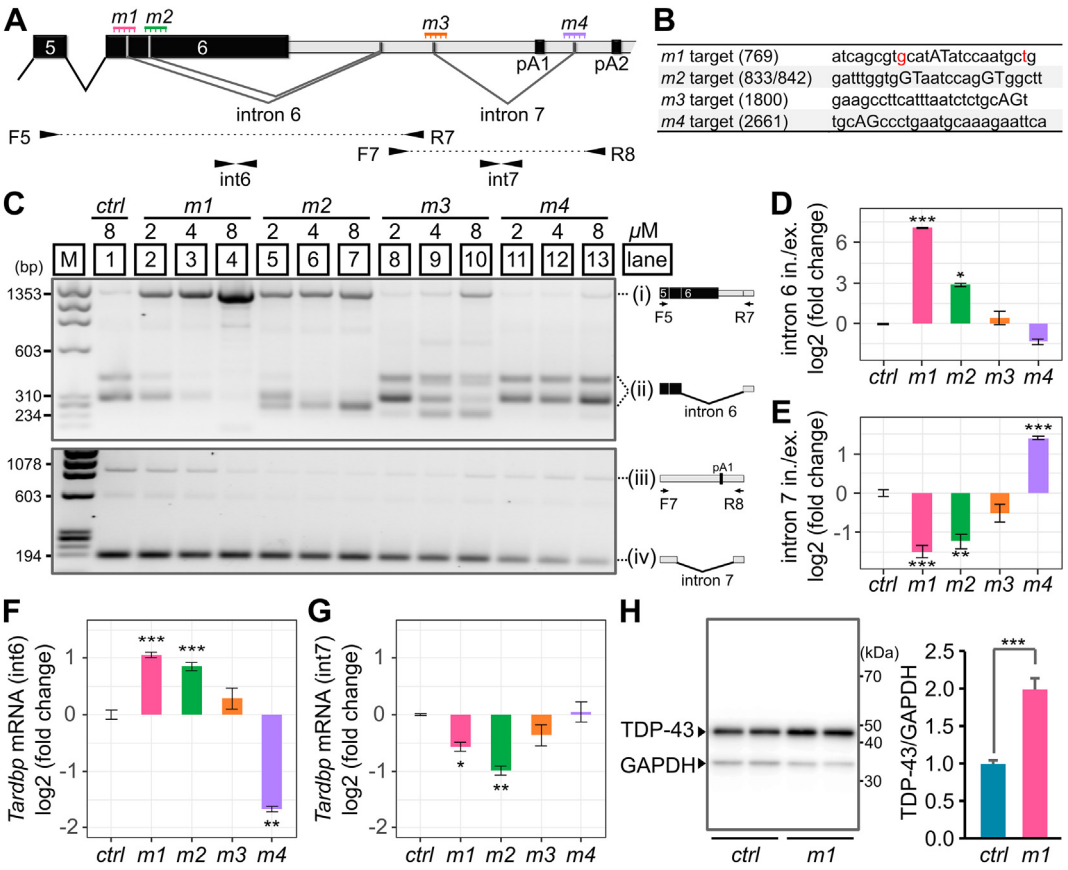


**Fig. 1. Inhibition of cryptic intron splicing of *Tardbp* mRNA in Neuro 2a cells.** (A) Schematic diagrams of *Tardbp* mRNA, target sites of ASO (m1, m2, m3, or m4), and primer positions of RT-PCR (F5/R7, F7/R8) and quantitative real-time PCR (int6, int7). (B) ASO target sequences. The capital letters represent cryptic intron splicing sites. The red letters indicate different human and mouse sequences. (C) RT-PCR analysis using F5/R7 primers (upper panel) and F7/R8 primers (lower panel) in Neuro 2a cells introduced with each ASO of each dose (2, 4, 8 μM). (D, E) The inclusion–exclusion ratio of each cryptic intron (D: cryptic intron 6; E: cryptic intron 7) when 8 μM ASO is introduced (mean ± SEM, n = 3). (F, G) Quantitative real-time PCR results of Neuro 2a cells introduced with 8 μM ASO using int6 primers (F) and int7 primers (G) normalized to *Gapdh* mRNA (mean ± SEM, n = 3). (H) Western blot analysis with anti-TDP-43 antibody and anti-GAPDH antibody of Neuro 2a cells introduced with 8 μM ASO and its quantitative analysis expressed as fold change compared to control (mean ± SEM, n = 4). *p < 0.05, **p < 0.01, ***p < 0.001; one-way ANOVA followed by Dunnett's test (D–G), or Student's *t* test (H).

serum albumin in PBS for 1 h and immersed in primary antibody at 4 °C overnight (rabbit anti-TDP-43 Ab, 1:3000, Proteintech 12892-1-AP; mouse anti-TUJ1 Ab, 1:3000, Abcam). Secondary antibody was used for 1 h at room temperature in the dark (Alexa Flour 568 goat anti-rabbit IgG antibody, 1:200; Alexa Fluor 488 goat anti-mouse IgG antibody, 1:200). Sections were incubated with autofluorescence eliminator reagent (Chemicon) for 5 min, washed with 70% ethanol and counterstained with DAPI. Images were taken with a BIOREVO BZ-9000 microscope (Keyence).

### 2.7. Quantification of the number of motor neurons

The lumbar spinal cord was excised and fixed with 4% paraformaldehyde. Fixed tissues were embedded in paraffin wax. Sections were made every 4 μm. One section was taken from every 25 sections, and a total of 12 sections were analyzed per mouse. Nissl-stained sections were imaged with a BIOREVO BZ-9000 microscope (Keyence). The number of cells with an area of 250 $\mu m^2$ or more in the anterior horn on one side of each section was counted using ImageJ software (1.49 v, National Institutes of Health, USA).

### 2.8. iPSC-derived neurons

To obtain normal human matured neuronal cells in a culture system, ReproNeuro, a neuron progenitor derived from human induced pluripotent stem cell (iPSC), was purchased from ReproCELL (Yokohama, Japan). For immunostaining and RNA analysis, the neural progenitor cells were seeded in a black clear bottom 96-well imaging plate (BD Biosciences) coated with ReproNeuro Coat solution (ReproCELL) and maintained in ReproNeuro maturation medium for 14 days according to the manufacturer's instructions. For western blot analysis, the neural progenitor cells were similarly seeded in a 12-well plate ($3 \times 10^5$ cells/well). Fourteen days after seeding, morpholino ASO and Endo-Porter were introduced into the medium at final concentrations of 10 μM and 2 μM, respectively.

### 2.9. Immunocytochemistry for iPSC-derived neurons

Cells were fixed with 3.7% formaldehyde preheated at 37 °C for 10 min and permeabilized with 0.1% Triton X-100 for 5 min. Cells were blocked with 5% bovine serum albumin for 30 min and stained with primary antibody for 1 h at room temperature (rabbit anti-TDP-43 Ab, 1:300, Proteintech 12892-1-AP; mouse anti-TUJ1 Ab, 1:500, Abcam). Secondary antibody was used at room temperature for 1 h in the dark (Alexa Flour 568 goat anti-rabbit IgG antibody, 1:300; Alexa Fluor 488 goat anti-mouse IgG antibody, 1:500). Cells were counterstained with Hoechst 33342. Images were taken with a BIOREVO BZ-9000 microscope (Keyence). The signal intensity of nuclear TDP-43 in 500 randomly selected TUJ-1 positive cells per well was measured with ImageJ software (1.49 v).

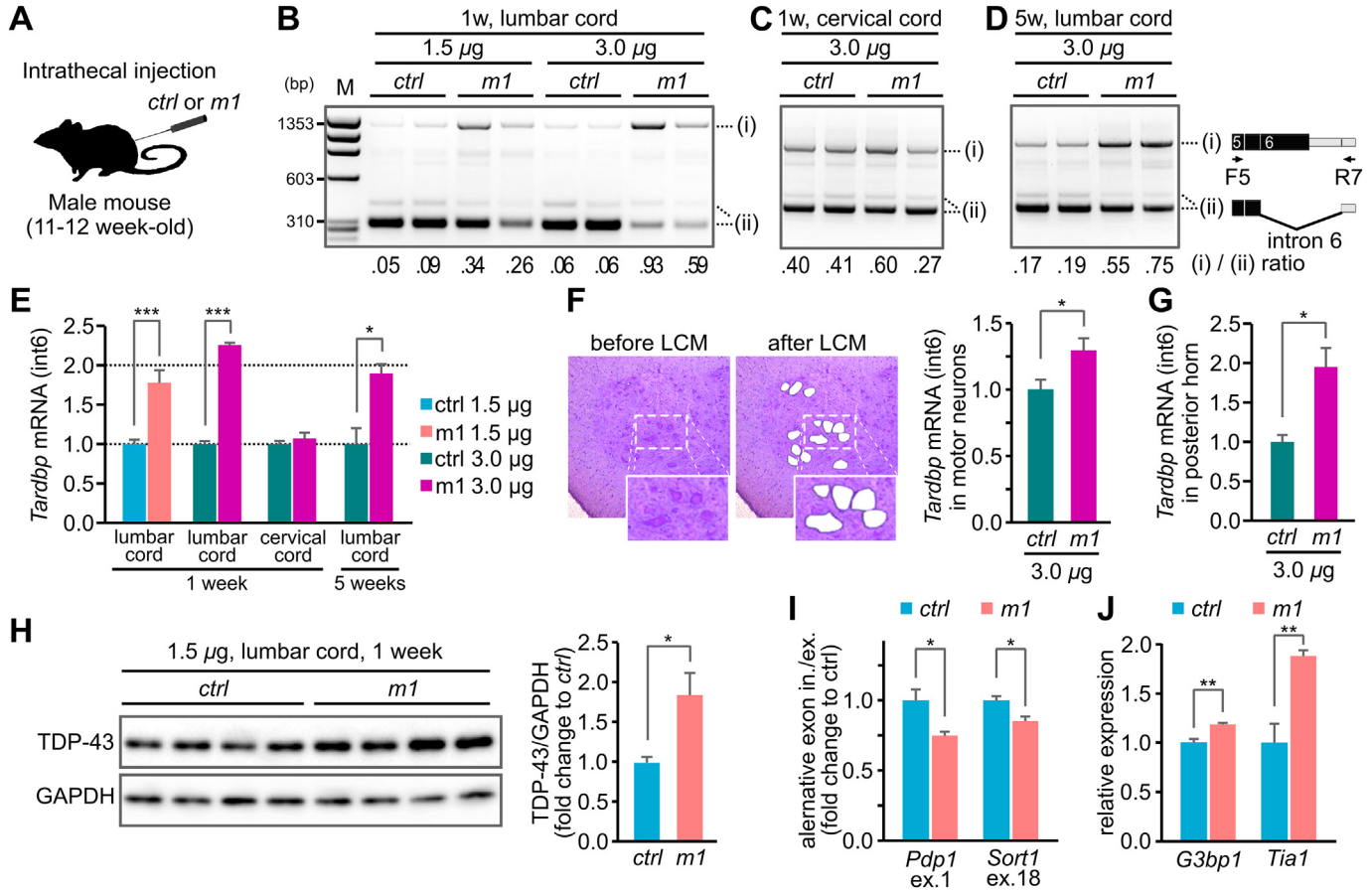


**Fig. 2. Overexpression of endogenous TDP-43 and target RNA metabolism in mouse spinal cord.** (A) Vivo-Morpholino (1.5 μg or 3.0 μg) was slowly injected into the intrathecal space of male mice (11–12 weeks old). (B, C, D) RT-PCR analysis of *Tardbp* mRNA by F5/R7 primers (Fig. 1A) in the lumbar (B) and cervical (C) cord 7 days after the injection, and in the lumbar cord 5 weeks after the injection (D). (E) Quantitative real-time PCR analysis of *Tardbp* mRNA that retains cryptic intron 6 normalized to *Gapdh* mRNA (mean ± SEM, $n = 4$). (F, G) Quantitative real-time PCR analysis of *Tardbp* mRNA that retains cryptic intron 6 normalized to *Gapdh* mRNA in the captured motor neurons (F) and in the captured posterior horns (G) (mean ± SEM, $n = 4$). (H) Western blot analysis of spinal cord (1.5 μg injection) with anti-TDP-43 antibody and anti-GAPDH antibody and its quantitative analysis expressed as fold change compared to control (mean ± SEM, $n = 4$). (I) Inclusion-exclusion ratios of exon 1 of *Pdp1* mRNA and exon 18 of *Sort1* mRNA semi-quantitated by RT-PCR analysis were expressed as fold change to control (mean ± SEM, $n = 4$). (J) Quantitative real-time PCR of *G3bp1* mRNA and *Tia1* mRNA normalized to *Gapdh* mRNA (mean ± SEM, $n = 4$). *p < 0.05, **p < 0.01, ***p < 0.001; Student's t test.

### 2.10. Protein extraction from iPSC-derived neurons and western blotting

Nuclear and cytoplasmic fraction of iPSC-derived neurons were extracted using NE-PER Nuclear and Cytoplasmic Extraction Reagents (Thermo). Western blotting was performed as described above. The amount of TDP-43 in the nuclear and cytoplasmic fraction was corrected by the amount of Lamin B1 and GAPDH, obtained by reprobing, respectively. Antibodies used for immunoblotting were rabbit anti-TDP-43 (C-Terminal) polyclonal antibody (Proteintech 12892-1-AP), rabbit anti-Lamin B1 polyclonal antibody (MBL), and mouse anti-GAPDH monoclonal antibody (MBL).

## 3. Results

### 3.1. Inhibition of splicing of cryptic intron increases TDP-43

To investigate the influence of autoregulation dysfunction, we sought to inhibit the alternative splicing of the cryptic introns of *TARDBP* pre-mRNA using antisense oligonucleotides (ASO). In a previous report, we showed that the inhibition of cryptic intron 6 splicing by introducing nucleotide substitutions at the splicing sites increases the canonical *TARDBP* mRNA (Koyama et al., 2016). The inhibition of cryptic intron 7 splicing inhibited cryptic intron 6 splicing, but not the reverse (Koyama et al., 2016). We therefore designed ASO to target the splicing sites of each cryptic intron (Fig. 1A). Cryptic intron 6 has three donor sites (cDNA nucleotide positions 769, 833, and 842 in human *TARDBP*) (Koyama et al., 2016). ASO-m1, ASO-m2, ASO-m3, and ASO-m4 were designed to target the donor site 769 for cryptic intron 6, both donor site 833 and 842 for cryptic intron 6, the donor site for cryptic intron 7, and the acceptor site for cryptic intron 7, respectively (Fig. 1A-B).

We first introduced each ASO (m1, m2, m3, m4, or ctrl) in Neuro 2a cells (mouse neuroblastoma cells) and investigated the alternative splicing of *Tardbp* mRNA after 48 h. ASO-m1 markedly inhibited the splicing of cryptic intron 6 and increased the canonical *Tardbp* mRNA (Fig. 1C, lane 4, Fig. 1D). ASO-m2 inhibited the splicing of cryptic intron 6, while inducing aberrant splicing around cryptic intron 6 (Fig. 1C, lanes 5-7). These ASOs did not inhibit the splicing of cryptic intron 7 (Fig. 1C, lanes 2-7), and conversely decreased the mRNA retaining intron 7 (Fig. 1E and G). ASO-m4 inhibited the splicing of cryptic intron 7 (Fig. 1C, lanes 11-13; Fig. 1E), but did not inhibit the splicing of cryptic intron 6 (Fig. 1C, lanes 11-13; Fig. 1D). ASO-m1 increased canonical *Tardbp* mRNA retaining cryptic intron 6 up to more than twice of the control ASO (ASO-ctrl) (Fig. 1F). Western blot analysis showed that ASO-m1 increased the amount of TDP-43 protein by approximately 2-fold (Fig. 1H).

We then investigated the functional consequence of increasing TDP-43. TDP-43 binds to *Pdp1* pre-mRNA and *Sort1* pre-mRNA and induces splicing out of exon 1 of *Pdp1* mRNA and exon 18 of *Sort1* mRNA (Supp. Fig. 1A and 1D) (Polymenidou et al., 2011; Ricketts et al., 2014). We therefore investigated the amounts of mRNA retaining these exons. ASO-m1 decreased *Pdp1* mRNA retaining exon 1 (Supp. Fig. 1B-C). ASO-m1 also decreased *Sort1* mRNA retaining exon 18, but not significantly (Supp. Fig. 1E-F). Immunofluorescence imaging confirmed that TDP-43 protein remained mostly nuclear, which was consistent with the result indicating enhancement of functional nuclear TDP-43 (Supp. Fig. 1G). We therefore concluded that the inhibition of cryptic intron 6 splicing of *Tardbp* mRNA increased functional TDP-43 and altered RNA metabolism.

### 3.2. Inhibition of splicing of the cryptic intron of Tardbp increases endogenous TDP-43 in the spinal cord

To address whether turbulence of the autoregulation mechanism increases TDP-43 and causes ALS-related pathology *in vivo*, we injected ASO (Vivo-Morpholinos: ASO-m1 or ASO-ctrl) into the lumbar intrathecal space of the 11 to 12-week-old male mouse (Fig. 2A). Seven days after injection, we investigated the splicing of *Tardbp* mRNA in the spinal cord. In the lumbar spinal cord, as expected, ASO-m1 reduced splicing of cryptic intron 6 and increased the canonical *Tardbp* mRNA in a dose-dependent manner (Fig. 2B). Under the injection of 3.0 μg of ASO-m1, the level of canonical *Tardbp* mRNA increased more than 2-fold compared to ASO-ctrl (Fig. 2E). Moreover, this splicing inhibitory effect was maintained even 5 weeks after administration (Fig. 2D and E). By contrast, the ASO effect did not reach the cervical spinal cord (Fig. 2C and E); therefore, we analyzed only the lumbar spinal cord in the following experiments. In the lumbar spinal cord, the amount of canonical *Tardbp* mRNA increased both in spinal motor neurons and posterior horn (Fig. 2F and G). TDP-43 protein increased in the lumbar spinal cord under the injection of 1.5 μg of ASO-m1 (Fig. 2H).

To investigate whether increasing endogenous TDP-43 alters RNA metabolism *in vivo*, we investigated the amounts of *Pdp1* mRNA retaining exon 1 and *Sort1* mRNA retaining exon 18 (Polymenidou et al., 2011; Ricketts et al., 2014). These mRNA decreased under injection of 1.5 μg of ASO-m1 (Fig. 2I). We also investigated the expression levels of *G3bp1* and *Tia1*, which encode the proteins associated with stress granules and are altered by TDP-43 (McDonald et al., 2011). The expression levels of *G3bp1* and *Tia1* were increased under 1.5 μg ASO-m1 treatment (Fig. 2J). These results indicate that ASO-m1 increases functional TDP-43 in mouse spinal cord.

### 3.3. Inhibition of splicing of cryptic intron 6 induced fragmentation of TDP-43

ASO-m1 inhibited the splicing of cryptic intron 6 and increased the expression level of *Tardbp* mRNA in a dose-dependent manner in mouse spinal cord (Fig. 2B and E). Indeed, an increase in TDP-43 protein was observed under the injection of 1.5 μg ASO-m1 (Fig. 2H). Unexpectedly, however, injection of 3.0 μg ASO-m1 reduced the ratio of the amount of RIPA soluble 43 kDa TDP-43 protein to *Tardbp* mRNA expression level (Fig. 3A-B). Instead, the injection of 3.0 μg of ASO-m1 increased urea-soluble 43 kDa TDP-43 and fragmented TDP-43 (35 kDa TDP-43; Fig. 3A and C). An antibody targeting 260-414 amino acids detected 35 kDa TDP-43, but an antibody targeting 1-260 amino acids did not detect it (Fig. 3A). Although it has been reported that alternative splicing within exon 2 produces 35 kDa species (Xiao et al., 2015), in this experimental model, alternative splicing within exon 2 did not change (Supp. Fig. 2A-B). Therefore, 35 kDa TDP-43 was concluded to be a C-terminal fragment. These results indicate that an excessive expression of endogenous TDP-43 causes fragmentation of TDP-43 and induces full-length TDP-43 into the insoluble fraction, resulting in a decrease in canonical soluble TDP-43.

### 3.4. Inhibition of splicing of cryptic intron 6 induced a loss of spinal motor neurons

It has been reported that the TDP-43 C-terminal fragment is cytotoxic in a cultured cell and increases the pro-apoptotic protein BIM (Bcl2111) (Igaz et al., 2009; Suzuki et al., 2011). We therefore investigated the BIM and number of neurons in the mouse spinal cord. Expression levels of *Bim* mRNA and the amount of BIM protein increased in the mouse spinal cord seven days after injection of 3.0 μg of ASO-m1 (Supp. Fig. 3A-D). Although *Bim* pre-mRNA is a TDP-43 target RNA and its alternative splicing is altered by a decrease in TDP-43 (Tollervey et al., 2011), ASO-m1 increased all isoforms of *Bim* mRNA (Supp. Fig. 3B). Furthermore, after 5 weeks of ASO injection, the number of motor neurons in the lumbar anterior horn decreased (Fig. 3D). At this time, motor symptoms are unclear and a disappearance of nuclear TDP-43 or cytoplasmic TDP-43 inclusion bodies was not observed by immunohistochemical analysis (Fig. 3E).

We then attempted to increase the effect of inhibition of cryptic intron splicing by modifying other factors. The activity of proteasome, which degrades TDP-43, is decreased in aged rodents (Keller et al., 2000; Tashiro et al., 2012). We have shown with an *in silico* model that decreasing the degradation efficiency also induces TDP-43 pathology (Sugai et al., 2018). We therefore investigated the effects of inhibition of cryptic intron splicing in elderly mice three weeks after injection of ASO-m1. We injected 17 to 18-month-old mice with 1.5 μg of ASO-m1, which did not induce TDP-43 fragmentation in 11 to 12-week-old mice. Both 43 kDa TDP-43 and 35 kDa TDP-43 showed an increasing trend, but not significantly (Supp. Fig. 4A-B). However, *Bim* mRNA and BIM protein both increased significantly (Supp. Fig. 4C-D). Moreover, the number of motor neurons in the lumbar anterior horn decreased (Supp. Fig. 4E).

### 3.5. Inhibition of cryptic intron 6 splicing decreased nuclear TDP-43 in human iPSC-derived neurons

We next inhibited splicing of cryptic intron 6 in human neuronal cells. To inhibit cryptic intron 6, we designed three ASOs to target its donor site (Fig. 4A; m1.1, m1.2, and m1.3). In HEK293T cells, we found that although all ASOs effectively inhibited the splicing of the cryptic intron (Fig. 4B), ASO-m1.3 most selectively inhibited the splicing of cryptic intron 6 without inducing aberrant splicing (Fig. 4B; arrowhead); we therefore used ASO-m1.3 in the following experiments.

We transfected ASO into the mature neurons derived from human induced pluripotent stem cells (iPSC; Fig. 4C), followed by analysis of these neurons after 7 and 14 days. Similar to the mouse spinal cord, we found that ASO-m1.3 inhibited alternative splicing of the cryptic intron and increased *TARDBP* mRNA that retains cryptic intron 6 (Fig. 4D–E). The expression of pro-apoptotic protein *BIM* mRNA was also increased in neurons at 7 days after transfection with ASO (Supp. Fig. 5).

Next, we investigated the subcellular localization of TDP-43 in the iPSC-derived neurons in which *TARDBP* mRNA was increased in the neurons at 7 days after transfection with ASO-m1.3. Western blotting showed that level of nuclear TDP-43 was decreased, whereas the cytoplasmic TDP-43 amount did not change in these neurons (Fig. 4F-H). We were not able to find fragmentation of TDP-43 (Fig. 4F). At 14 days after transfection with ASO, we found a few neurons with a disappearance of nuclear TDP-43 by fluorescent immunohistochemistry analysis (Fig. 4I). By comparing the TDP-43 intensities in the nucleus, we noticed that a group with low fluorescence intensity in nuclear TDP-43 existed in the neurons transfected with ASO-m1.3 (Fig. 4J). The percentage of neurons with a fluorescence intensity Z score of $-1.96$ or less in nuclear TDP-43, which indicates decreased nuclear TDP-43, was higher in the neurons transfected with ASO-m1.3 compared to the control neurons (Mean [SD], 3.9 [1.7] % vs. 0.2 [0.4] %, $t = -5.21$, $p = 0.003$) (Fig. 4K). On the other hand, there was no difference in the percentage of neurons with a Z score of 1.96 or more in nuclear TDP-43

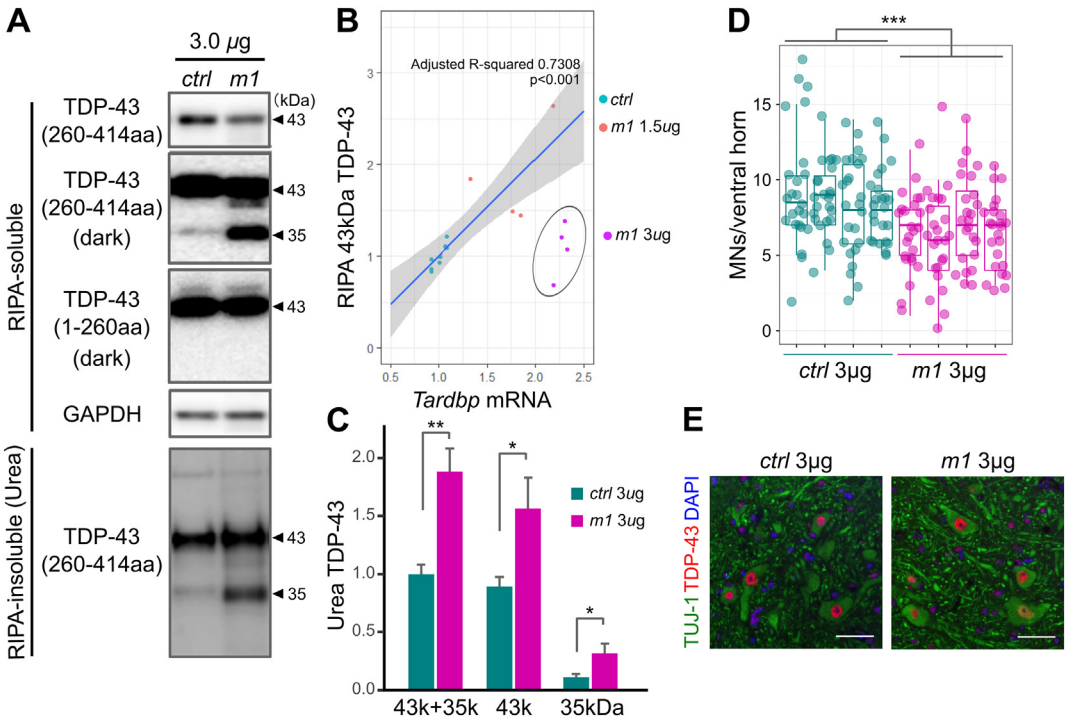


**Fig. 3. Fragmentation of TDP-43 and relative decrease of functional TDP-43.** (A) Western blotting of RIPA soluble fraction or urea soluble fraction from spinal cord 7 days after intrathecal injection of 3.0 μg of Vivo-Morpholinos. (B) The correlation of expression of *Tardbp* mRNA and RIPA soluble 43 kDa TDP-43 amount obtained from the spinal cord of mice administered with ASO-ctrl and ASO-m1 1.5 μg, but not ASO-m1 3.0 μg, is shown. (C) 43 kDa and 35 kDa TDP-43 in urea fraction were expressed as fold change to control (mean ± SEM, $n = 3$–4, *$p < 0.05$, **$p < 0.01$; Student's *t* test). (D) The numbers of motor neurons greater than 250 $\mu m^2$ at the ventral horn on one side of each section of the lumbar spinal cord 5 weeks after administration of 3.0 μg of Vivo-Morpholinos are shown. (E) Immunofluorescence analysis of the lumbar spinal cord performed 5 weeks after administration of 3.0 μg of Vivo-Morpholinos. Green indicates TUJ 1, red indicates TDP-43, and blue indicates DAPI. Scale bar indicates 40 μm. *$p < 0.05$, ***$p < 0.001$; Student's *t* test.

fluorescence intensity (Fig. 4K).

## 4. Discussion

In this study, we showed that the inhibition of cryptic intron 6 splicing of *TARDBP* mRNA increased the amount of canonical *TARDBP* mRNA and TDP-43 protein in mouse spinal cord and canonical *TARDBP* mRNA in iPSC-derived human neurons. A prominent increase of endogenous TDP-43 had been difficult due to the robust autoregulation system of the amount of TDP-43. However, the inhibition of cryptic intron splicing converted NMD-susceptible transcripts to canonical ones and increased *TARDBP* mRNA expression up to 2-fold. These results suggest that the transcriptional redundancy of *TARDBP* mRNA is also present in mouse spinal cord and human neurons.

Regarding the autoregulation mechanism of TDP-43, we and others have proposed that the splicing of cryptic intron 6 takes a crucial role (Koyama et al., 2016; Polymenidou et al., 2011). A mechanism independent of cryptic intron 6 splicing—without producing NMD-susceptible mRNA—has also been proposed (Avendaño-Vázquez et al., 2012; Ayala et al., 2011). Both hypotheses have been proposed by a forced expression system using cultured cell lines, and the dynamics of *TARDBP* mRNA in the neuron *in vivo* have therefore not been fully elucidated. Our results reveal that inhibition of cryptic intron 6 splicing increased canonical *TARDBP* mRNA in mouse spinal cord and iPSC-derived human neurons. These results support our hypothesis that the splicing of cryptic intron 6 is crucial for autoregulation of TDP-43 (Koyama et al., 2016; Polymenidou et al., 2011).

An increase in fragmented TDP-43 in the insoluble fraction and a decrease in nuclear TDP-43 are biochemical features in ALS (Kabashi et al., 2008; Neumann et al., 2006; Rutherford et al., 2008). The present study shows an increase in C-terminal fragments of TDP-43 in the insoluble fraction *in vivo* upon increasing the amount of endogenous canonical *Tardbp* mRNA. This finding is consistent with previous results, which state that forced expression of exogenous TDP-43 leads to generation of fragmented TDP-43 (Tsai et al., 2010; Xu et al., 2010). Moreover, the alternative splicing inhibition by ASO caused a relative decline in soluble full-length TDP-43 in the mouse spinal cord. In the human iPSC-derived neurons, the splicing inhibition also lessened the nuclear TDP-43 despite no change in cytoplasmic TDP-43 amount; causing a marked decrease in nuclear TDP-43 in some neurons, as shown by immunostaining. We did not demonstrate the mechanism by which nuclear TDP-43 decreases despite increased *TARDBP* mRNA expression in human iPSC-derived neurons. Nevertheless, based on indirect evidence, we speculate that an elevation in TDP-43 production causes endoplasmic reticulum (ER) stress with increased BIM expression (Suzuki et al., 2011), which induces impaired nuclear translocation and fragmentation of TDP-43 (Walker et al., 2013). In normal human cells, full-length TDP-43 degrades faster in the cytoplasm than in the nucleus (Scotter et al., 2014; Watanabe et al., 2013), and fragmented TDP-43 degrades much faster than full-length TDP-43 (Scotter et al., 2014). These mechanisms maintaining TDP-43 protein homeostasis may contribute to the discrepancy between levels of *TARDBP* mRNA and TDP-43 protein in human neurons (Li et al., 2015; Yin et al., 2019).

In mouse motor neurons, the alternative splicing inhibition by ASO did not recapitulate ALS-related TDP-43 pathology including loss of nuclear TDP-43 with cytoplasmic inclusions. This could be attributed to a possible limitation of this study, wherein the mice only up to 5 weeks after ASO introduction were subjected to investigation. A longer wait may be necessary for the formation of inclusion bodies, as it has been shown that a decrease in nuclear TDP-43 and an increase in insoluble TDP-43 precedes the formation of inclusion bodies (Brandmeir et al., 2008; Mori et al., 2008). To test this possibility, it is necessary to develop a method to introduce ASO that maintains its effect over a longer period. Meanwhile, other factors besides the ASO administration

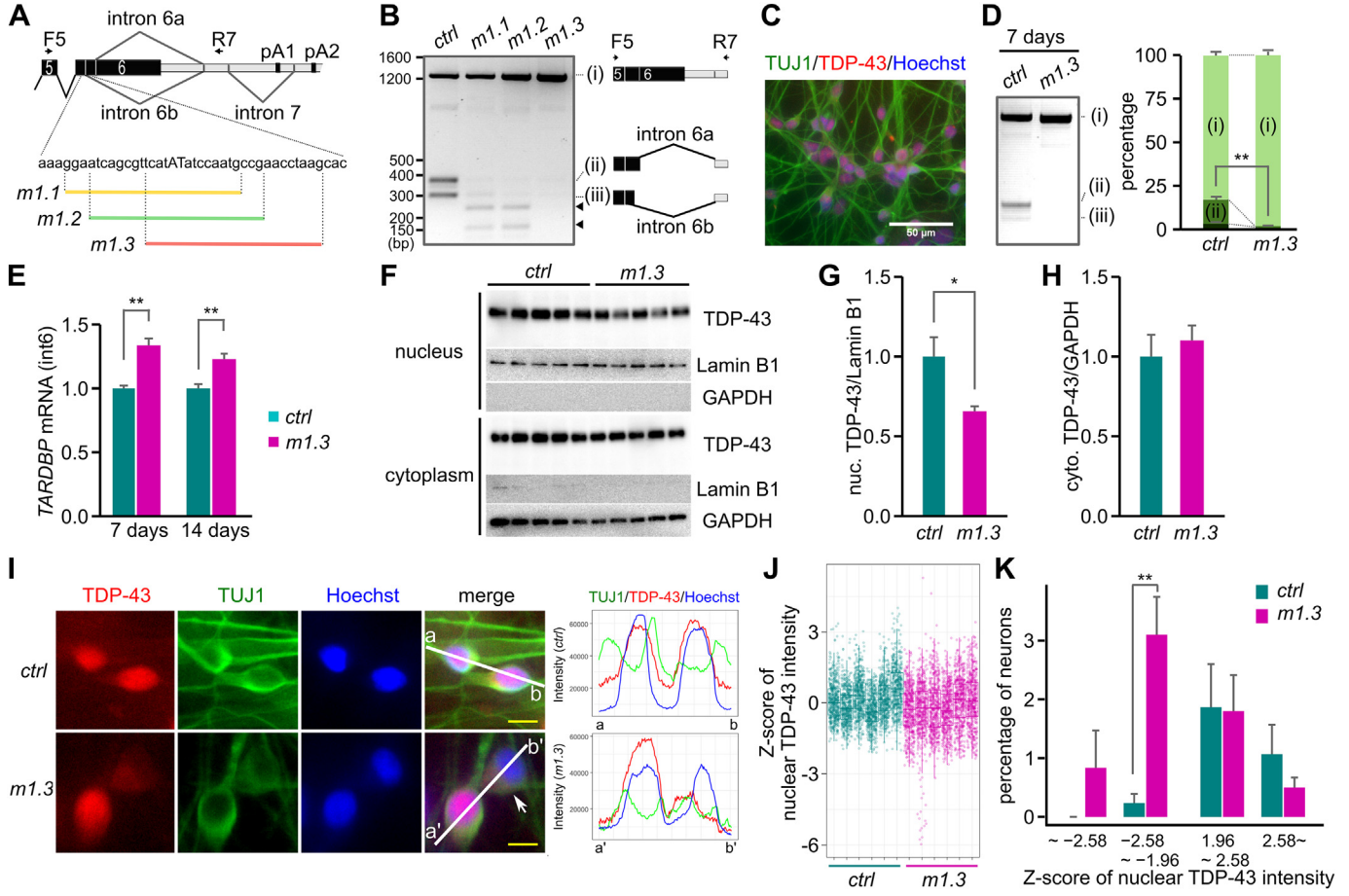


**Fig. 4. Decreased nuclear TDP-43 by disorder of autoregulation in iPSC-derived neurons.** (A) ASO target sites to inhibit alternative splicing of human *TARDBP* mRNA (m1.1, m1.2, and m1.3). (B) Alternative splicing of *TARDBP* mRNA using F5/R7 primers in HEK293T cells 48 h after introduction of ASO. (C) Representative image before ASO introduction of human iPSC-derived neurons stained with anti-TUJ1 antibody (green), anti-TDP-43 antibody (red), and Hoechst 33342 (blue). (D) RT-PCR analysis with F5/R7 primers 7 days after introduction of ASO-ctrl or ASO-m1.3 in iPSC-derived neurons and the percentage of each isoform obtained by semi-quantifying each band (mean ± SEM, $n = 3$). (E) Expression level of canonical *TARDBP* mRNA that retains cryptic intron 6 at 7 and 14 days after introduction of ASO by quantitative real-time PCR analysis normalized to *GAPDH* mRNA (mean ± SEM, $n = 4$). (F) Western blotting on nuclear and cytoplasmic fraction of iPSC-derived neurons 7 days after introduction of ASO. Lamin B1 and GAPDH are loading control of nuclear and cytoplasmic fraction, respectively. (G, H) The amount of nuclear TDP-43 relative to Lamin B1 (G) and cytoplasmic TDP-43 relative to GAPDH (H) are shown (mean ± SEM, n = 5). (I) Representative image showing localization of TDP-43 in neurons into which ASO was introduced and intensity of each fluorescence on line ab (or line a'b'). Scale bar indicates 10 μm. (J) Z score of nuclear TDP-43 intensity of each iPSC-derived neurons 14 days after introduction of ASO-ctrl or ASO-1.3. (K) Percentage of neurons classified by the Z score of nuclear TDP-43 intensity of neurons into which ASO-ctrl or ASO-m1.3 was introduced (mean ± SEM, $n = 6$). *p < 0.05, **p < 0.01; Student's *t* test.

period, such as species differences between mice and humans, may have to be considered. While carrying out the revision for this manuscript, the primate-specific ER membrane-bound caspase-4, but not the mouse homologue caspase-11, was reported to generate fragmented TDP-43 and reduce full-length TDP-43 by exogenous TDP-43 overexpression (Yin et al., 2019). In addition, consistent with our experimental mouse model, *Tardbp* knock-in mouse with an ALS-causative gene mutation did not show TDP-43 pathology despite the increase in endogenous TDP-43 with decreased alternative splicing (White et al., 2018). Therefore, recapitulating ALS-related TDP-43 pathology by inhibition of *Tardbp* alternative splicing might be species dependent.

The inhibition of cryptic intron 6 splicing reduced the number of motor neurons in the mouse spinal cord. This neuronal loss by excessive endogenous TDP-43 is consistent with the findings of several mouse models overexpressing exogenous TDP-43 (Tsai et al., 2010; Xu et al., 2010). Although we did not demonstrate the neurons that led to apoptosis, we speculate that an increase in BIM, a core factor in the neuron-specific JNK-mediated apoptotic pathway, contributes to this phenomenon to some extent. In motor neurons, loss of BIM protects from motor neuron death in SOD1 transgenic mice (Soo et al., 2012). BIM is induced by increased TDP-43 C-terminal fragment or ER stress (Puthalakath et al., 2007; Suzuki et al., 2011). We therefore speculate that insoluble fragmented TDP-43 protein itself—or elicited ER stress—increases BIM and induces neuronal cell death. In addition, the loss of canonical TDP-43 can also cause motor neuron death by interfering with RNA metabolism (Ishihara et al., 2013; Shiga et al., 2012; Tollervey et al., 2011).

Interestingly, the *TARDBP* mutation associated with ALS accumulates around cryptic intron 6. Indeed, motor neurons derived from iPSC obtained from ALS patients with *TARDBP* mutation showed increased TDP-43 (Egawa et al., 2012). Moreover, the ALS mice harboring a mutation in cryptic intron 6 increased the amount of *Tardbp* mRNA and caused neuronal cell death (Fratta et al., 2018; White et al., 2018). It would be interesting to investigate whether these mutations alter the splicing of cryptic intron 6 and autoregulation of TDP-43. Trans-acting factors in splicing control should also be noted, however. Splicing is regulated by several RNA binding proteins. The alteration of these splicing factors could disturb the autoregulation of TDP-43, resulting in TDP-43 pathology. Indeed, abnormal localization and expression of RNA-binding proteins have been reported in ALS (Bakkar et al., 2017). Moreover, mutations of the splicing factors also cause familial ALS (Kim et al., 2013). These mutant splicing factors may alter TDP-43

autoregulation. Studies of TDP-43 dynamics according to changes in each of these factors may provide a new angle for elucidating the pathogenesis of ALS.

In conclusion, this study showed that a decrease in alternative splicing efficiency increases *TARDBP* mRNA and increases insoluble and fragmented TDP-43, resulting in a decrease in soluble TDP-43. Overproduction of TDP-43 is based on transcriptional redundancy of *TARDBP*. Therefore, the optimal intervention on the processing of *TARDBP* transcripts may conversely reduce insoluble and fragmented TDP-43 with restore of nuclear TDP-43 (Sugai et al., 2018). To prove this repair process, an animal model holding the TDP-43 autoregulation system must be used. Despite the need to improve the duration and extent of the ASO effect, the method without genetic modification in this study suggests a novel strategy for creating a model for sporadic neurodegenerative diseases.

## Acknowledgements

This research was supported by a grant-in-aid for Scientific Research on Innovative Areas (Brain Protein Aging and Dementia Control; 26117006) from MEXT; grants-in-aid for Scientific Research (A) (26250017 and 25253065) and a grant-in-aid for Scientific Research (C) (17K09751) from the Japan Society for the Promotion of Science; a grant-in-aid from the Research Committee of CNS Degenerative Diseases and Comprehensive Research on Disability, Health, and Welfare (13230021) from the Japanese Ministry of Health, Labour, and Welfare of Japan; and a grant-in-aid from the Takeda Science Foundation.

## Author contributions

AS and OO designed this study and wrote the paper. AS conducted experiments and analyzed the results. TKA and AK contributed to preliminary experiments. YK contributed to experiments using iPSC-derived neurons. TKO and TI contributed to the interpretation of the results. All authors critically revised the draft and approved the final version.

## Declaration of Competing Interests

The authors declare no competing interests.

## Appendix A. Supplementary data

Supplementary data to this article can be found online at https://doi.org/10.1016/j.nbd.2019.104534.

## References

Arai, T., Hasegawa, M., Akiyama, H., Ikeda, K., Nonaka, T., Mori, H., Mann, D., Tsuchiya, K., Yoshida, M., Hashizume, Y., Oda, T., 2006. TDP-43 is a component of ubiquitin-positive tau-negative inclusions in frontotemporal lobar degeneration and amyotrophic lateral sclerosis. Biochem. Biophys. Res. Commun. 351, 602–611. https://doi.org/10.1016/j.bbrc.2006.10.093.

Avendaño-Vázquez, S.E., Dhir, A., Bembich, S., Buratti, E., Proudfoot, N., Baralle, F.E., 2012. Autoregulation of TDP-43 mRNA levels involves interplay between transcription, splicing, and alternative polyA site selection. Genes Dev. 26, 1679–1684. https://doi.org/10.1101/gad.194829.112.

Ayala, Y.M., De Conti, L., Avendaño-Vázquez, S.E., Dhir, A., Romano, M., D'Ambrogio, A., Tollervey, J., Ule, J., Baralle, M., Buratti, E., Baralle, F.E., 2011. TDP-43 regulates its mRNA levels through a negative feedback loop. EMBO J. 30, 277–288. https://doi.org/10.1038/emboj.2010.310.

Bakkar, N., Kovalik, T., Lorenzini, I., Spangler, S., Lacoste, A., Sponaugle, K., Ferrante, P., Argentinis, E., Sattler, R., Bowser, R., 2017. Artificial intelligence in neurodegenerative disease research: use of IBM Watson to identify additional RNA-binding proteins altered in amyotrophic lateral sclerosis. Acta Neuropathol. 135, 1–21. https://doi.org/10.1007/s00401-017-1785-8.

Brandmeir, N.J., Geser, F., Kwong, L.K., Zimmerman, E., Qian, J., Lee, V.M.Y., Trojanowski, J.Q., 2008. Severe subcortical TDP-43 pathology in sporadic frontotemporal lobar degeneration with motor neuron disease. Acta Neuropathol. 115, 123–131. https://doi.org/10.1007/s00401-007-0315-5.

Egawa, N., Kitaoka, S., Tsukita, K., Naitoh, M., Takahashi, K., Yamamoto, T., Adachi, F., Kondo, T., Okita, K., Asaka, I., Aoi, T., Watanabe, A., Yamada, Y., Morizane, A., Takahashi, J., Ayaki, T., Ito, H., Yoshikawa, K., Yamawaki, S., Suzuki, S., Watanabe, D., Hioki, H., Kaneko, T., Makioka, K., Okamoto, K., Takuma, H., Tamaoka, A., Hasegawa, K., Nonaka, T., Hasegawa, M., Kawata, A., Yoshida, M., Nakahata, T., Takahashi, R., Marchetto, M.C.N., Gage, F.H., Yamanaka, S., Inoue, H., 2012. Drug screening for ALS using patient-specific induced pluripotent stem cells. Sci. Transl. Med. 4, ra104. https://doi.org/10.1126/scitranslmed.3004052.

Fratta, P., Sivakumar, P., Humphrey, J., Lo, K., Ricketts, T., Oliveira, H., Brito-Armas, J.M., Kalmar, B., Ule, A., Yu, Y., Birsa, N., Bodo, C., Collins, T., Conicella, A.E., Mejia Maza, A., Marrero-Gagliardi, A., Stewart, M., Mianne, J., Corrochano, S., Emmett, W., Codner, G., Groves, M., Fukumura, R., Gondo, Y., Lythgoe, M., Pauws, E., Peskett, E., Stanier, P., Teboul, L., Hallegger, M., Calvo, A., Chiò, A., Isaacs, A.M., Fawzi, N.L., Wang, E., Housman, D.E., Baralle, F., Greensmith, L., Buratti, E., Plagnol, V., Fisher, E.M., Acevedo-Arozena, A., 2018. Mice with endogenous TDP-43 mutations exhibit gain of splicing function and characteristics of amyotrophic lateral sclerosis. EMBO J. 37, e98684. https://doi.org/10.15252/embj.201798684.

Igaz, L.M., Kwong, L.K., Chen-plotkin, A., Winton, M.J., Unger, T.L., Xu, Y., Neumann, M., Trojanowski, J.Q., Lee, V.M.-Y., 2009. Expression of TDP-43 C-terminal fragments in vitro recapitulates pathological features of TDP-43 proteinopathies. J. Biol. Chem. 284, 8516–8524. https://doi.org/10.1074/jbc.M809462200.

Ishihara, T., Ariizumi, Y., Shiga, A., Kato, T., Tan, C.-F., Sato, T., Miki, Y., Yokoo, M., Fujino, T., Koyama, A., Yokoseki, A., Nishizawa, M., Kakita, A., Takahashi, H., Onodera, O., 2013. Decreased number of Gemini of coiled bodies and U12 snRNA level in amyotrophic lateral sclerosis. Hum. Mol. Genet. 22, 4136–4147. https://doi.org/10.1093/hmg/ddt262.

Kabashi, E., Valdmanis, P.N., Dion, P., Spiegelman, D., McConkey, B.J., Vande Velde, C., Bouchard, J.-P., Lacomblez, L., Pochigaeva, K., Salachas, F., Pradat, P.-F., Camu, W., Meininger, V., Dupre, N., Rouleau, G. a, 2008. *TARDBP* mutations in individuals with sporadic and familial amyotrophic lateral sclerosis. Nat. Genet. 40, 572–574. https://doi.org/10.1038/ng.132.

Ke, Y.D., van Hummel, A., Stevens, C.H., Gladbach, A., Ippati, S., Bi, M., Lee, W.S., Krüger, S., van der Hoven, J., Volkerling, A., Bongers, A., Halliday, G., Haass, N.K., Kiernan, M., Delerue, F., Ittner, L.M., 2015. Short-term suppression of A315T mutant human TDP-43 expression improves functional deficits in a novel inducible transgenic mouse model of FTLD-TDP and ALS. Acta Neuropathol. 130, 661–678. https://doi.org/10.1007/s00401-015-1486-0.

Keller, J.N., Huang, F.F., Markesbery, W.R., 2000. Decreased levels of proteasome activity and proteasome expression in aging spinal cord. Neuroscience 98, 149–156. https://doi.org/10.1016/S0306-4522(00)00067-1.

Kim, H.J., Kim, N.C., Wang, Y.D., Scarborough, E.A., Moore, J., Diaz, Z., MacLea, K.S., Freibaum, B., Li, S., Molliex, A., Kanagaraj, A.P., Carter, R., Boylan, K.B., Wojtas, A.M., Rademakers, R., Pinkus, J.L., Greenberg, S.A., Trojanowski, J.Q., Traynor, B.J., Smith, B.N., Topp, S., Gkazi, A.S., Miller, J., Shaw, C.E., Kottlors, M., Kirschner, J., Pestronk, A., Li, Y.R., Ford, A.F., Gitler, A.D., Benatar, M., King, O.D., Kimonis, V.E., Ross, E.D., Weihl, C.C., Shorter, J., Taylor, J.P., 2013. Mutations in prion-like domains in hnRNPA2B1 and hnRNPA1 cause multisystem proteinopathy and ALS. Nature 495, 467–473. https://doi.org/10.1038/nature11922.

Koyama, A., Sugai, A., Kato, T., Ishihara, T., Shiga, A., Toyoshima, Y., Koyama, M., Konno, T., Hirokawa, S., Yokoseki, A., Nishizawa, M., Kakita, A., Takahashi, H., Onodera, O., 2016. Increased cytoplasmic *TARDBP* mRNA in affected spinal motor neurons in ALS caused by abnormal autoregulation of TDP-43. Nucleic Acids Res. 44, 5820–5836. https://doi.org/10.1093/nar/gkw499.

Li, Q., Yokoshi, M., Okada, H., Kawahara, Y., 2015. The cleavage pattern of TDP-43 determines its rate of clearance and cytotoxicity. Nat. Commun. 6, 6183. https://doi.org/10.1038/ncomms7183.

Ling, S.-C., Polymenidou, M., Cleveland, D.W., 2013. Converging mechanisms in ALS and FTD: disrupted RNA and protein homeostasis. Neuron 79, 416–438. https://doi.org/10.1016/j.neuron.2013.07.033.

McDonald, K.K., Aulas, A., Destroismaisons, L., Pickles, S., Beleac, E., Camu, W., Rouleau, G. a, Vande Velde, C., 2011. TAR DNA-binding protein 43 (TDP-43) regulates stress granule dynamics via differential regulation of G3BP and TIA-1. Hum. Mol. Genet. 20, 1400–1410. https://doi.org/10.1093/hmg/ddr021.

Mori, F., Tanji, K., Zhang, H.X., Nishihira, Y., Tan, C.F., Takahashi, H., Wakabayashi, K., 2008. Maturation process of TDP-43-positive neuronal cytoplasmic inclusions in amyotrophic lateral sclerosis with and without dementia. Acta Neuropathol. 116, 193–203. https://doi.org/10.1007/s00401-008-0396-9.

Neumann, M., Sampathu, D.M., Kwong, L.K., Truax, A.C., Micsenyi, M.C., Chou, T.T., Bruce, J., Schuck, T., Grossman, M., Clark, C.M., McCluskey, L.F., Miller, B.L., Masliah, E., Mackenzie, I.R., Feldman, H., Feiden, W., Kretzschmar, H. a, Trojanowski, J.Q., Lee, V.M.-Y., 2006. Ubiquitinated TDP-43 in frontotemporal lobar degeneration and amyotrophic lateral sclerosis. Science 314, 130–133. https://doi.org/10.1126/science.1134108.

Polymenidou, M., Lagier-tourenne, C., Hutt, K.R., Stephanie, C., Moran, J., Liang, T.Y., Ling, S.-C., Sun, E., Wancewicz, E., Mazur, C., Kordasiewicz, H., Sedaghat, Y., Paul, J., Shiue, L., Bennett, C.F., Yeo, G.W., Cleveland, D.W., Huelga, S.C., Donohue, J.P., 2011. Long pre-mRNA depletion and RNA missplicing contribute to neuronal vulnerability from loss of TDP-43. Nat. Neurosci. 14, 459–468. https://doi.org/10.1038/nn.2779.

Puthalakath, H., Reilly, L.A.O., Gunn, P., Lee, L., Kelly, P.N., Huntington, N.D., Hughes, P.D., Michalak, E.M., Mckimm-breschkin, J., Motoyama, N., Gotoh, T., Akira, S., Bouillet, P., Strasser, A., 2007. ER stress triggers apoptosis by activating BH3-only protein Bim. Cell 129, 1337–1349. https://doi.org/10.1016/j.cell.2007.04.027.

Ratti, A., Buratti, E., 2016. Physiological functions and pathobiology of TDP-43 and FUS/TLS proteins. J. Neurochem. 138, 95–111. https://doi.org/10.1111/jnc.13625.

Ricketts, T., McGoldrick, P., Fratta, P., de Oliveira, H.M., Kent, R., Phatak, V., Brandner,

S., Blanco, G., Greensmith, L., Acevedo-Arozena, A., Fisher, E.M.C., 2014. A nonsense mutation in mouse Tardbp affects TDP43 alternative splicing activity and causes limb-clasping and body tone defects. PLoS One 9, e85962. https://doi.org/10.1371/journal.pone.0085962.

Rutherford, N.J., Zhang, Y., Baker, M., Gass, J.M., Finch, N. a, Xu, Y.-F., Stewart, H., Kelley, B.J., Kuntz, K., Crook, R.J.P., Sreedharan, J., Vance, C., Sorenson, E., Lippa, C., Bigio, E.H., Geschwind, D.H., Knopman, D.S., Mitsumoto, H., Petersen, R.C., Cashman, N.R., Hutton, M., Shaw, C.E., Boylan, K.B., Boeve, B., Graff-Radford, N.R., Wszolek, Z.K., Caselli, R.J., Dickson, D.W., Mackenzie, I.R., Petrucelli, L., Rademakers, R., 2008. Novel mutations in *TARDBP* (TDP-43) in patients with familial amyotrophic lateral sclerosis. PLoS Genet. 4, e1000193. https://doi.org/10.1371/journal.pgen.1000193.

Scotter, E.L., Vance, C., Nishimura, A.L., Lee, Y.-B., Chen, H.-J., Urwin, H., Sardone, V., Mitchell, J.C., Rogelj, B., Rubinsztein, D.C., Shaw, C.E., 2014. Differential roles of the ubiquitin proteasome system and autophagy in the clearance of soluble and aggregated TDP-43 species. J. Cell Sci. 127, 1263–1278. https://doi.org/10.1242/jcs.140087.

Shiga, A., Ishihara, T., Miyashita, A., Kuwabara, M., Kato, T., Watanabe, N., Yamahira, A., Kondo, C., Yokoseki, A., Takahashi, M., Kuwano, R., Kakita, A., Nishizawa, M., Takahashi, H., Onodera, O., 2012. Alteration of POLDIP3 splicing associated with loss of function of TDP-43 in tissues affected with ALS. PLoS One 7, e43120.

Soo, K.Y., Atkin, J.D., Farg, M., Walker, A.K., Horne, M.K., Nagley, P., 2012. Bim links ER stress and apoptosis in cells expressing mutant SOD1 associated with amyotrophic lateral sclerosis. PLoS One 7, e35413. https://doi.org/10.1371/journal.pone.0035413.

Sreedharan, J., Blair, I.P., Tripathi, V.B., Hu, X., Vance, C., Rogelj, B., Ackerley, S., Durnall, J.C., Williams, K.L., Buratti, E., Baralle, F., de Belleroche, J., Mitchell, J.D., Leigh, P.N., Al-Chalabi, A., Miller, C.C., Nicholson, G., Shaw, C.E., 2008. TDP-43 mutations in familial and sporadic amyotrophic lateral sclerosis. Science 319, 1668–1672. https://doi.org/10.1126/science.1154584.

Sugai, A., Kato, T., Koyama, A., Koike, Y., Kasahara, S., Konno, T., Ishihara, T., Onodera, O., 2018. Robustness and vulnerability of the autoregulatory system that maintains nuclear TDP-43 levels: a trade-off hypothesis for ALS pathology based on in silico data. Front. Neurosci. 12, 28. https://doi.org/10.3389/FNINS.2018.00028.

Suzuki, H., Lee, K., Matsuoka, M., 2011. TDP-43-induced death is associated with altered regulation of BIM and Bcl-xL and attenuated by caspase-mediated TDP-43 cleavage. J. Biol. Chem. 286, 13171–13183. https://doi.org/10.1074/jbc.M110.197483.

Tashiro, Y., Urushitani, M., Inoue, H., Koike, M., Uchiyama, Y., Komatsu, M., Tanaka, K., Yamazaki, M., Abe, M., Misawa, H., Sakimura, K., Ito, H., Takahashia, R., 2012. Motor neuron-specific disruption of proteasomes, but not autophagy, replicates amyotrophic lateral sclerosis. J. Biol. Chem. 287, 42984–42994. https://doi.org/10.1074/jbc.M112.417600.

Tollervey, J.R., Curk, T., Rogelj, B., Briese, M., Cereda, M., Kayikci, M., König, J., Hortobágyi, T., Nishimura, A.L., Zupunski, V., Patani, R., Chandran, S., Rot, G., Zupan, B., Shaw, C.E., Ule, J., 2011. Characterizing the RNA targets and position-dependent splicing regulation by TDP-43. Nat. Neurosci. 14, 452–458. https://doi.org/10.1038/nn.2778.

Tsai, K.-J., Yang, C.-H., Fang, Y.-H., Cho, K.-H., Chien, W.-L., Wang, W.-T., Wu, T.-W., Lin, C.-P., Fu, W.-M., Shen, C.-K.J., 2010. Elevated expression of TDP-43 in the forebrain of mice is sufficient to cause neurological and pathological phenotypes mimicking FTLD-U. J. Exp. Med. 207, 1661–1673. https://doi.org/10.1084/jem.20092164.

Walker, A.K., Soo, K.Y., Sundaramoorthy, V., Parakh, S., Ma, Y., Farg, M.a., Wallace, R.H., Crouch, P.J., Turner, B.J., Horne, M.K., Atkin, J.D., 2013. ALS-associated TDP-43 induces endoplasmic reticulum stress, which drives cytoplasmic TDP-43 accumulation and stress granule formation. PLoS One 8, e81170. https://doi.org/10.1371/journal.pone.0081170.

Walker, A.K., Spiller, K.J., Ge, G., Zheng, A., Xu, Y., Zhou, M., Tripathy, K., Kwong, L.K., Trojanowski, J.Q., Lee, V.M.-Y.M.Y., 2015. Functional recovery in new mouse models of ALS/FTLD after clearance of pathological cytoplasmic TDP-43. Acta Neuropathol. 130, 643–660. https://doi.org/10.1007/s00401-015-1460-x.

Watanabe, S., Kaneko, K., Yamanaka, K., 2013. Accelerated disease onset with stabilized familial amyotrophic lateral sclerosis (ALS)-linked mutant TDP-43 proteins. J. Biol. Chem. 288, 3641–3654. https://doi.org/10.1074/jbc.M112.433615.

White, M.A., Kim, E., Duffy, A., Adalbert, R., Phillips, B.U., Peters, O.M., Stephenson, J., Yang, S., Massenzio, F., Lin, Z., Andrews, S., Segonds-Pichon, A., Metterville, J., Saksida, L.M., Mead, R., Ribchester, R.R., Barhomi, Y., Serre, T., Coleman, M.P., Fallon, J., Bussey, T.J., Brown Jr., R.H., Sreedharan, J., 2018. TDP-43 gains function due to perturbed autoregulation in a Tardbp knock-in mouse model of ALS-FTD. Nat. Neurosci. 21, 552–563. https://doi.org/10.1038/s41593-018-0113-5.

Xiao, S., Sanelli, T., Chiang, H., Sun, Y., Chakrabartty, A., Keith, J., Rogaeva, E., Zinman, L., Robertson, J., 2015. Low molecular weight species of TDP-43 generated by abnormal splicing form inclusions in amyotrophic lateral sclerosis and result in motor neuron death. Acta Neuropathol. 130, 49–61. https://doi.org/10.1007/s00401-015-1412-5.

Xu, Y.-F., Gendron, T.F., Zhang, Y.-J., Lin, W.-L., D'Alton, S., Sheng, H., Casey, M.C., Tong, J., Knight, J., Yu, X., Rademakers, R., Boylan, K., Hutton, M., McGowan, E., Dickson, D.W., Lewis, J., Petrucelli, L., 2010. Wild-type human TDP-43 expression causes TDP-43 phosphorylation, mitochondrial aggregation, motor deficits, and early mortality in transgenic mice. J. Neurosci. 30, 10851–10859. https://doi.org/10.1523/JNEUROSCI.1630-10.2010.

Yin, P., Guo, X., Yang, W., Yan, S., Yang, S., Zhao, T., Sun, Q., Liu, Y., Li, S., Li, X.-J., 2019. Caspase-4 mediates cytoplasmic accumulation of TDP-43 in the primate brains. Acta Neuropathol. https://doi.org/10.1007/s00401-019-01979-0.

Yokoseki, A., Shiga, A., Tan, C.-F., Tagawa, A., Kaneko, H., Koyama, A., Eguchi, H., Tsujino, A., Ikeuchi, T., Kakita, A., Okamoto, K., Nishizawa, M., Takahashi, H., Onodera, O., 2008. TDP-43 mutation in familial amyotrophic lateral sclerosis. Ann. Neurol. 63, 538–542. https://doi.org/10.1002/ana.21392.

Zhou, H., Janghra, N., Mitrpant, C., Dickinson, R.L., Anthony, K., Price, L., Eperon, I.C., Wilton, S.D., Morgan, J., Muntoni, F., 2013. A novel morpholino oligomer targeting ISS-N1 improves rescue of severe spinal muscular atrophy transgenic mice. Hum. Gene Ther. 24, 331–342. https://doi.org/10.1089/hum.2012.211.